Where does the river end? Drivers of spatiotemporal variability in CO_2 concentration and flux in the inflow area of a large boreal lake

Hannah E. Chmiel[1,2,*], Hilmar Hofmann[3], Sebastian Sobek[4], Tatyana Efremova[5], and Natacha Pasche[1,2]

[1] Limnology Center, EPFL-ENT-LIMNC, Lausanne, 1015, Switzerland
[2] Physics of Aquatic Systems Laboratory, Margaretha Kamprad Chair, EPFL-ENAC-IEE-APHYS, 1015 Lausanne, Switzerland
[3] Environmental Physics Group, University of Konstanz, Limnological Institute, 78464 Konstanz, Germany
[4] Department of Ecology and Genetics, Limnology, Uppsala University, 75236 Uppsala, Sweden
[5] Northern Water Problems Institute, Karelian Research Centre, Russian Academy of Sciences, 185030 Petrozavodsk, Russia

Email contacts:

hannah.chmiel@epfl.ch *corresponding author*

hilmar.hofmann@uni-konstanz.de

sebastian.sobek@ebc.uu.se

efremova.nwpi@mail.ru

natacha.tofield-pasche@epfl.ch

Keywords: carbon dioxide emission, ice-melt period, river intrusion

Abstract

River inflow affects the spatiotemporal variability of carbon dioxide (CO_2) in the water column of lakes and may locally influence CO_2 gas exchange with the atmosphere. However, spatiotemporal CO_2 variability at river inflow sites is often unknown leaving estimates of lake-wide CO_2 emission uncertain. Here, we investigated the CO_2 concentration and flux variability along a river-impacted bay and remote sampling locations of Lake Onego. During three years, we resolved spatial CO_2 gradients between river inflow and central lake and recorded the temporal course of CO_2 in the bay from the ice-covered period to early summer. We found that the river had a major influence on the spatial CO_2 variability during ice-cover periods and contributed ~35% to the total amount of CO_2 in the bay. The bay was a source of CO_2 to the atmosphere at ice-melt each year emitting 2-15 times the amount as an equally-sized area in the central lake. However, there was large interannual variability in the spring CO_2 emission from the bay related to differences in discharge and climate that affected the hydrodynamic development of the lake during spring. In early summer, the spatial CO_2 variability was unrelated to the river signal but correlated negatively with dissolved oxygen concentrations instead indicating a stronger biological control on CO_2. Our study reveals a large variability of CO_2 and its drivers at river inflow sites at the seasonal and at the interannual time scale. Understanding these dynamics is essential for predicting lake-wide CO_2 fluxes more accurately under a warming climate.

Introduction

Lakes and rivers are dynamics sites of carbon transport and processing and, at the global scale, a net source of carbon dioxide (CO_2) to the atmosphere (Cole et al. 2007, Tranvik et al. 2009; Aufdenkampe et al. 2011). Despite covering about five times less area on land than lakes and reservoirs, it is estimated that rivers and streams contribute up to 85% to the annual inland water CO_2 emission flux, indicating their disproportionally high influence for water-atmosphere CO_2 gas exchange (Cole et al. 2007, Raymond et al. 2013, Lauerwald et al. 2015). Global estimates of net aquatic CO_2 release range between 0.8 and 2.1 Pg C yr^{-1}, however, there are large uncertainties associated with these estimates (Cole et al. 2007, Raymond et al. 2013). While these are partly related to the challenge of accurately estimating global inland water area, there is furthermore a lack of information on spatial and temporal variability not only in CO_2 flux but also in its environmental drivers (Verpoorter et al. 2014; Hastie et al. 2017; Klaus et al. 2019). Large extends in this variability might be expected at the interface of lentic and lotic systems, i.e., at river inflow areas, which might add comparatively large uncertainty to whole-system CO_2 flux estimates. However, only limited information on CO_2 dynamics exist for these sites, although the hydrological contribution to CO_2 in lakes has been pointed out frequently (Schilder et al. 2013; Pacheco et al. 2015; Natchimuthu et al. 2017).

The reason why rivers and streams are on average more supersaturated in CO_2 than lakes, is their higher connection with the terrestrial environment along their margins (Raymond et al. 2013; Crawford et al. 2014). Fluvial export of dissolved organic carbon (DOC) from soils, which is partly mineralized to CO_2 during transport, as well as direct inputs of CO_2 from soil respiration both contribute to supersaturation and net emission of stream CO_2 into the atmosphere (Jones and Mulholland 1998; Worrall and Lancaster 2005; Öquist et al. 2009; Wallin et al. 2013; Crawford et al. 2014). In this context, it has been shown that fluvial export can also account for considerable fractions of excess CO_2 in lakes (Maberly et al. 2013; Chmiel et al. 2016), which indicates that the transition zone from rivers to lakes are probably important and highly dynamic hot spots for lake CO_2 emission. Since aquatic CO_2 concentrations are controlled by biological activity, water chemistry, and physical transport processes, their dynamics at inflow areas will be complex and vary with temporal changes in river discharge and lake hydrodynamics. In large systems with heterogeneous basin morphology and confined water circulation, substantial gradients in CO_2 might develop, such that a lack in information on spatial CO_2 variability might considerable bias whole-systems CO_2 flux assessments (Kelly et al. 2001; Paranaíba et al. 2018).

A lot of scientific effort has been dedicated to CO_2 flux dynamics in boreal aquatic ecosystems (Rantakari and Kortelainen 2005; Einola et al. 2011; Teodoru et al. 2011; Weyhenmeyer et al. 2012; Denfeld et al. 2015a). The boreal forest region is considered as one of the most important carbon (C) sinks on land; however, the high density of inland waters in this landscape counteracts this terrestrial C sink (Intergovernmental Panel on Climate Change (IPCC) 2013; Verpoorter et al. 2014; Lauerwald et al. 2015; Hastie et al. 2017). A large source of uncertainty in CO_2 emission from these systems arises from the period of ice-melt in spring and early summer. Boreal lakes typically experience ice-cover during substantial parts of the year; and it is anticipated that the sudden release of accumulated CO_2 at ice-melt accounts for a considerable proportion of the total annual CO_2 flux into the atmosphere (Weyhenmeyer et al. 2011; Karlsson et al. 2013; Jones et al. 2016). However, only a few studies have resolved temporal CO_2 trends under ice and quantified CO_2 emission flux at ice breakup based on direct *in-situ* measurements (Baehr and Degrandpre 2002, 2004; Denfeld et al. 2015a). These studies have demonstrated that the bio-physical environment under ice can be complex, such that large uncertainty remains about the extends and mechanisms of interannual CO_2 flux variability at ice-melt (Denfeld et al. 2018).

In this study, we investigated the impact of river inflow on the spatiotemporal variability in CO_2 concentration and flux in the second largest lake of Europe, Lake Onego (Republic of Karelia, Russia). During three successive years, we resolved vertical and horizontal gradients in, CO_2, DOC and dissolved inorganic carbon (DIC) concentrations and CO_2 fluxes between a river-impacted bay and the central lake area before and after the period of ice-melt. Furthermore, quantified the contribution of sediment and river CO_2 fluxes to under-ice CO_2 accumulation and monitored the partial pressure of CO_2 (pCO_2) in the bay to assess temporal trends of CO_2 from the ice-covered to the open water period and to quantify the CO_2 emission flux at ice-melt. We hypothesized that (1) spatial, seasonal and interannual CO_2 variability would be greater in the river-impacted bay than in the central lake (2) and that the bay would exhibit consistently higher CO_2 concentrations and fluxes to the atmosphere than the central lake due to the river inflow.

Methods

Study site

Lake Onego is located in western Russia and extends between 60.9-62.9°N and 34.3-36.5°E with a surface area of 9720 km^2. The lake has a mean and maximum depth of 30 and 127 m, respectively,

and its basin shape is defined by several elongated bays in its northern and a large central main basin in its southern part (Fig. 1). While Lake Onego is overall classified as an oligotrophic system, several of the bays exhibit meso- to eutrophic conditions related to human impacts in their watersheds (Sabylina et al. 2010; Efremova et al. 2019). The ice-cover season of Lake Onego typically lasts from December to mid-April (Filatov et al. 2019). River inflow into Lake Onego is provided through 52 large rivers (>10 km length) and more than 1150 smaller tributaries that deliver a total water volume of 13-28 km^3 per year (Sabylina et al. 2010). The Shuya river is the second largest tributary that drains a 10'300 km^2 catchment of ~70 % boreal forest and ~30 % wetlands and lakes and delivers 23 % of the total annual discharge (Lozovik et al. 2007; Sabylina et al. 2010). The Shuya river water enters the lake through the lake's easternmost bay, the Bay of Petrozavodsk (PB), which has a surface area of 73 km^2 and a mean and maximum water depth of 16 and 27 m, respectively, and which is considered mesotrophic (Table 1; Sabylina et al. 2010; Efremova et al. 2019). Highest discharge is usually recorded from April to May during the spring melt season and lowest discharge from January to March, when the lake is ice-covered (Filatov et al. 2019).

Field campaigns

In 2015-2017, six sampling campaigns were carried out on Lake Onego with three campaigns taking place in March, when the lake was ice-covered and three campaigns taking place in early June, when the lake was ice-free. In addition, water samples were retrieved biweekly from the river mouth from February to May 2016 in order to resolve temporal changes in CO_2 concentration. The entire lake area enclosed in this study covered about 270 km2 in the western part of the lake including the PB area. Sampling points in the bay followed a transect from the Shuya river mouth towards the central lake, whereas, transects during the open water season in the central lake varied to some extend between years depending on the cruise of the research vessel. Maximum water depths over all sampling stations varied from 5 m at the river mouth to 84 m in the central lake (Fig.1).

CO_2, DIC, and DOC sampling and analysis

To obtain the vertical and horizontal distribution of dissolved CO_2, dissolved inorganic carbon (DIC) and dissolved organic carbon (DOC) concentrations, water samples were taken at each station (Fig. 1) with a customized Ruttner sampler. At the river inflow, samples were retrieved from 0.5 m depth. Within the bay area, water samples for vertical profiles were obtained from up to five different locations with a depth resolution of 2-3 m starting at the lake surface. In the central lake, up to three different locations were sampled for vertical profiles and the depth resolution varied between 4 and

15 m, depending on the maximum water depth. In addition to the vertical profiles, water samples were retrieved from the lake surface along two transects in June 2016 (TS, TB) and one transect (T0) in June 2017, with a horizontal spacing of about 1-2 km between sampling points.

Samples for CO_2 were analysed as described by Sobek et al. (2003). Triplicates of each water sample were immediately transferred into 60 ml syringes, which were filled bubble-free, and adjusted to a volume of 30 ml. A headspace of 30 ml ambient air was added to each syringe and ambient air was collected in addition in separate syringes to correct for atmospheric CO_2. The gas and water phase were then equilibrated by shaking the syringes for 2 min, and the pCO_2 in the headspace was measured with a portable infrared gas analyser (EGM-4, Environmental Gas Analyser). In addition to CO_2, we also analysed the inorganic carbon (DIC) concentration, which followed the same procedure, except that a 20 ml water volume in the syringe was acidified with 100 µL of diluted hydrochloric acid (HCl, 3.7%) and a headspace of 40 ml was added. Both CO_2 and DIC concentrations in the water were calculated via Henry's constant (Weiss 1974) after correction for the atmospheric pressure and the amount of CO_2 added to the headspace volume from the ambient air.

For analysing the dissolved organic carbon (DOC) concentration, water was filtered through pre-rinsed 0.45 µm cellulose membrane filter, acidified with HCl 3.7%, and kept at 4°C until analysis in the laboratory at EAWAG (Switzerland) using a Shimadzu TOC-L.

In-situ measurements of CO_2 and abiotic conditions

To measure the temporal course in CO_2 near the ice cover and near the lake bottom over the ice-melt period, two CO_2 sensors (ProOceanus Mini CO_2^{TM}, range: 0-5000 µatm, accuracy: ± 100 µatm), were deployed at the bay centre in March 2015 and 2016 (Fig. 1, point IC). In 2015, the water depths corresponded to 3 m and 25 m, and in 2016 to 4.5 m and 26 m, respectively. The logger recorded pCO_2 at hourly intervals until retrieval in early June in each of the years. Sensors were calibrated before and after each campaign and data corrected for drift (0.5% per month).

In addition, temperature was recorded every 30 minutes on a separate mooring. In 2015, thermistors (RBRsolo) were installed at 5 and 25 m water depth about 50 m away from the CO_2 mooring. In 2016, temperature sensors (T-RBR and Vemco) were deployed on the CO_2 mooring, in equal

distances of 2 m between 4 and 26 m water depth. During sampling campaigns in June, temperature and oxygen profiles were taken at each measurement site using CTD probes (Sea & Sun or RBRconcerto).

Sediment CO_2 flux experiments

In March 2016, nine sediment cores were retrieved from three different sides of Lake Onego in order to quantify the flux of CO_2 from sediment into water via incubation experiments (Supplementary Information, Table S1). The upper five cm of sediment and the overlying ~20 cm of water were immediately transferred to incubation cores, without disturbing the sediment. To avoid mixing during transportation of the samples, the lid of each incubation core, which contains a tubing, was carefully pressed to the sediment surface, so that the overlying water could be removed and collected in bottles. All samples were stored dark and cold during transportation and upon experiment start at the laboratory at Uppsala University, where cores were carefully re-filled with the respective lake water sample, via the tubing in the lid, and without creating any visible disturbance of the sediment. The incubations followed the method described in (Gudasz et al. 2010), where the CO_2 flux is determined as the rate of change in DIC concentration in the water volume overlying the sediment (see Supplementary Information).

River discharge, climate data and ice-breakup dates

Discharge data of the Shuya River were provided by the All-Russian Scientific Institute of Hydrometeorological Information, and were available for the period 1955-2017 as monthly mean values. Air temperature, precipitation and wind speed data from the meteorological station in Petrozavodsk were obtained from the open database at *http://rp5.ru* and available as three-hour mean values for the period February 2005 to December 2017. The period of ice-breakup in PB for the years 2015-2017 was estimated from climate and in-situ monitoring data (see section In-situ measurements of CO_2 and abiotic conditions) and validated by satellite images from LANCE-MODIS Terra, which were available on a daily basis (Supplementary Information, Fig. S2). In addition, air temperature, wind speed, and wind direction during early summer campaigns were also recorded from the meteorological station mounted on top of the research vessel.

CO_2 flux calculations

The diffusive flux of CO_2 between lake and atmosphere was calculated using the boundary layer model as described by *Liss & Slater* [1974]:

$$F_{CO2} = k_{CO2} \bullet M_{CO2} \bullet (C_w - C_{eq}) \quad (1)$$

where F_{CO_2} is the flux of CO_2 above the air-water interface in mmol m^{-2} h^{-1}, k_{CO_2} the transfer velocity of CO_2 in m h^{-1}, M_{CO_2} the molar mass of CO_2, C_w the measured near-surface water molar concentration of CO_2, and C_{eq} the molar concentration of CO_2 in the surface water that is in equilibrium with the atmospheric concentration at surface water temperatures. The transfer velocity of CO_2 was estimated at standard conditions k_{600} (Schmidt number 600) using the equation of *Liss & Merlivat* [1986]:

$$k_{CO2} = k_{600} \bullet (Sc\ /600)^n \quad (2)$$

where *Sc* is the Schmidt number (-) of CO_2 at water surface temperature (Wanninkhof 1992) and *n* is for wind speed $U_{10} \leq 3.7$ m s^{-1} and for $U_{10} > 3.7$ m s^{-1}. The gas transfer velocity k_{600} was calculated using the equation of *Cole & Caraco* [1998]:

$$k_{600} = 2.07 + 0.215 \bullet U_{10}^{1.7} \text{ cm } h^{-1} \quad (3)$$

and additionally from the equations by *Crusius & Wanninkhof* [2003]:

$$\text{for } U_{10} < 3.7 \text{ m } s^{-1}: \quad k_{600} = 0.72 \bullet U_{10} \text{ cm } h^{-1}$$

$$\text{for } U_{10} > 3.7 \text{ m } s^{-1}: \quad k_{600} = 4.33 \bullet U_{10} - 13.3 \text{ cm } h^{-1} \quad (4)$$

The C_{eq} of CO_2 was calculated according to *Wiesenburg & Guinasso* [1979], whereby the pCO_2 in the atmosphere was set to 397 µatm. For better comparability and to upscale CO_2 fluxes over the entire study area, we also calculated daily CO_2 fluxes (mmol m^{-2} d^{-1}) using the median recorded U_{10} (4 m s^{-1}) for all stations and dates. The deviation in flux values between the two k_{600} models was about 7% at this wind speed, and were reported as the mean value obtained from both of the two relationships.

The same approach was applied to the CO_2 sensor data to obtain CO_2 emission fluxes at ice-melt and lake overturn in 2015 and in 2016. In 2016, however, the sensor at 4.5 m water depth had stopped measuring just before ice breakup occurred. Therefore, CO_2 fluxes could only be estimated from the

227 data recorded at 26 m water depth during a short a period of complete mixing conditions (see
228 Supplementary Information).

229 ***Statistical analysis***

230 The sampling campaigns generated a spatial dataset of in total 349 CO_2 observations including 30
231 water column profiles and 71 surface water measurements obtained within 4-6 weeks before and after
232 ice melt each year. In addition, the sensor measurements from ice-cover to open water periods
233 revealed temporal records of in total 15 482 hourly pCO_2 measurements in the bay center.

234 For comparing CO_2 concentrations, water column profile data were interpolated over depth to
235 calculated mean values and the coefficient of variation (CV, %) for each profile. Mean CO_2
236 concentrations were non-normally distributed (Shapiro Wilk's test, $p<0.01$), therefore we used non-
237 parametric Wilcoxon test to evaluate differences in mean CO_2 concentrations between bay and central
238 lake as well as between seasons and between years. Furthermore, we tested whether CO_2
239 concentrations in the water column were correlated to DIC, DOC, and DO concentrations during the
240 different seasons. Seasonal trends within the river CO_2 dataset of 2016 dataset and *in-situ* CO_2
241 measurements (non-normally distributed, $p<0.0001$) were calculated by applying a Mann-Kendall
242 test to the different periods (ice-covered, break-up/mixing, and stratified period), where significant
243 increases and decreases in CO_2 concentration were calculated as the median slope (i.e., *Theil-Sen*
244 estimator) of multiple regression lines through pairs of data points. In addition, synchrony (S)
245 between surface and bottom water measurements was tested by pairwise cross-correlation of the time
246 series within each year, where high synchrony is indicated by values near 1 and low synchrony by
247 values near 0. Interannual variability in climate and discharge conditions in the PB area where
248 assessed from the two long-term datasets. We calculated mean air temperatures and precipitation for
249 the ice-melt periods and for the timespans between ice-breakup dates and the early June campaigns
250 as well as the 95% confidence intervals for the same periods of the preceding decade. Furthermore,
251 we tested for linear and non-linear relationships between discharge and precipitation data at the
252 monthly, seasonal and annual timescale. All analyses were performed in R (R Development Core
253 Team 2011) using the stats, mblm, Kendall, and synchrony packages.

Results

Variability in spring climate, discharge, ice breakup dates and lake stratification

The years 2015, 2016, and 2017 were the wettest on the 13-year record and showed 83-172 % higher amounts of precipitation from January to May, than the mean of the preceding decade (Supplementary Information, Fig. S3). However, discharge and precipitation did not reveal any clear relationships at monthly, seasonal and interannual time scale (Filatov et al. 2019). Discharge from January to June followed the long-term pattern (Fig. S2) with lowest values in March (25-48 m^3 s^{-1}) and highest values in May (223-335 m^3 s^{-1}). The intensity of discharge from January to March differed however between years, with a ~50% lower average rate in 2015 (29 ± 5 m^3 s^{-1}) than in 2016 (57 ± 5 m^3 s^{-1}) and in 2017 (58 ± 9 m^3 s^{-1}). The average discharge from April to June, in contrast, reached a similar intensity in 2015 and 2016 (171 ± 55 m^3 s^{-1}, 161 ± 36 m^3 s^{-1}), but was about 30% higher in 2017 (212 ± 72 m^3 s^{-1}).

Air temperatures differed considerably between the three years. In 2015 and 2016, mean air temperatures from March to mid-April were above the freezing point of 0 °C (1.3 and 0.2 °C), whereas spring in 2017 was considerably colder, with an average air temperature of -0.6 °C. This differences in spring air temperatures affected the timing of ice-breakup dates. In 2015 and 2016, the ice-started to crack in mid-April, however, while the total melt-process lasted only 3 days in 2015, it took about two weeks in 2016. In 2017, by contrast the complete ice-melt did not occur before the beginning of May (Figs. S2).

The timespan from the ice-breakup dates to the field campaigns in early June equaled 55, 40, and 30 days in 2015, 2016, and 2017, respectively; and air temperatures during these periods averaged 7.3 °C, 12.3 °C, and 5.0 °C. For comparison, the 95% CI air temperature range considering the same three periods over the preceding 10 years (2005-2014) were 6-8 °C, 8-9 °C, and 9-10 °C, which shows that the PB area experienced a relatively warm period after ice-break in 2016, and a relatively cold period in 2017 (Fig. S3). *In-situ* temperature records revealed a mixing period after ice-melt that lasted about 4 weeks in 2015, but only 8 days in 2016. By early June 2015 and 2016, the water column in the entire bay was thermally stratified, with surface water temperatures of 10-16 °C and 15-16 °C. Sampling points in the central lake revealed colder temperatures of 4 and 7 °C. The conditions in June 2017 differed considerably from the those of the two previous years, with surface water temperatures of 6-9 °C in the bay and 5-3 °C in the central lake. A thermal bar was observed 8 km outside the bay area, which separated the warmer water of the bay region from the still inversely

stratified open lake. This thermal 4 °C-front was observed between the bay and point C3 in 2017, while it was already ahead of point C2 in 2015 and 2016 (Fig. 2).

Spatiotemporal variability in CO_2 concentrations

CO_2 concentrations at the river mouth varied between 45 and 168 µmol L^{-1}. The lowest values (≤ 52 µmol L^{-1}) were obtained in early June, whereas all other sampling dates of the ice-covered periods and the spring melt season 2016 revealed CO_2 concentrations ≥ 105 µmol L^{-1}. The biweekly CO_2 dataset of the river mouth from 2016 indicated an overall decline in CO_2 concentrations from winter to early summer (Mann-Kendall's τ = -0.4, p<0.05, n=10, Supplementary Information, Fig. S6).

CO_2 concentrations in the lake varied between 1 and 276 µmol L^{-1} (pCO_2; 10-3892 µatm), with the lowest values observed in surface waters in the central basin in early June, and the highest values in bottom water layers of the bay during ice-covered periods. The bay showed overall a larger CO_2 concentration range (16-276 µmol L^{-1}) and a higher vertical CO_2 variability (median CV = 17 %) than the central basin (1-62 µmol L^{-1}; median CV = 10%; Figs. 2,3,4). There were strong seasonal changes in the spatial CO_2 variability of the bay. During ice-covered periods in 2016 and 2017, CO_2 maxima (> 100 µmol L^{-1}) were observed at intermediate water column depths and in bottom water layers near the sediment (Figs. 3 and 4). Horizontally, CO_2 concentrations decreased from the river mouth (120-131 µmol L^{-1}) towards the central basin (31-40 µmol L^{-1}). These horizontal gradients were less pronounced in early June, when CO_2 concentrations at the river mouth were 60% lower, and mean water column CO_2 concentrations in the bay 7-38% lower than in March (p<0.001). Furthermore, we found considerable interannual variability in CO_2 concentrations of the bay, where mean water column CO_2 concentration were significantly lower in 2015 than in 2016 and 2017. These differences were not observed in the central lake (Table 2).

The in-situ records at the bay center (Fig. 4) revealed an average (±SD) CO_2 concentration under ice of 65 ± 5 µmol L^{-1} at 3 m depth in 2015 (3 weeks of measurements) and of 98 ± 11 µmol L^{-1} at 4.5 m depth in 2016 (4 weeks of measurements). A positive trend of 1 µmol $L^{-1}d^{-1}$ was detected in 2015 (Mann-Kendall's τ=0.56, p<0.0001, n=431), however, no trend was detected for under-ice measurements in 2016 at 4.5 m depth. The deep water sensor data, provided a highly different pattern. In 2015, CO_2 concentrations at 25 m water depth, fluctuated strongly between 58-256 µmol L^{-1} varying about 7 times stronger (CV=49%) than CO_2 at 3 m water depth (CV=7%). Similarly, CO_2

concentrations varied strongly at 26 m depth in 2016 (76-257 μmol L^{-1}, CV = 23%), but revealed in addition a positive trend of 4 μmol $L^{-1}d^{-1}$ (34 days, τ = 0.60, p<0.0001, n=802).

During the 4-week mixing period in 2015, the CO_2 concentrations at 3 m and 25 m water depth showed a high synchrony (S=0.94; mean pairwise correlation: 0.88 for n=600) with a decrease of 2 μmol $L^{-1}d^{-1}$ (τ = -0.74 and -0.58, p<0.0001 and n=360 each) over the first two weeks. Thereafter, CO_2 concentration remained rather stable but started to, fluctuated in a more asynchronous manner in the two depth layers during stratified conditions (40 ± 3 μmol L^{-1} and 49 ± 6 μmol L^{-1}at 3 m and 25 m water depth).

In 2016, when the ice started to break in mid-April, CO_2 at 4.5 m sensor stopped measuring. At 26 m water depth, CO_2 decreased for two weeks at a rate of -12 μmol $L^{-1}d^{-1}$ (τ = 0.60, p<0.0001, n=802) and remained stable at about 88 ± 2 μmol L^{-1} for the 8-days mixing period. About one week after stratification was established, later, CO_2 concentration at 26 m water depth started to increase at a rate of 2 2 μmol $L^{-1}d^{-1}$ (τ = 0.77, p<0.0001, n=481) over about one months.

Relation of CO_2 with DOC and DIC and DO concentrations

DOC and DIC concentrations varied between 0.47-1.58 mmol L^{-1} and between 0.14-0.65 mmol L^{-1}, respectively (Table 2). Similar to CO_2, mean DOC concentrations in the bay were higher in 2016 and 2017 than in 2015, however, there was no difference in DOC concentrations between seasons. During ice-covered periods, CO_2 and DOC concentrations correlated positively; and the correlation was strongest when CO_2-rich bottom water layers were excluded from the relationship (R^2= 0.84, p<0.0001, n=59; Fig. S5). In early June, by contrast, DOC did not reveal any correlation with CO_2 (Supplementary Information, Fig. S8).

DIC concentrations did not differ between years, but exhibited seasonal differences. During ice-covered periods, DIC concentrations correlated negatively with CO_2 concentrations in the water column, excluding the bottom water layers (R^2= 0.38, p<0.0001, n=83; Fig. S7). In bottom waters, by contrast, CO_2 and DIC concentrations exhibited a strong positive correlation indicating a contribution of CO_2 from sediments into the lake water (R^2= 0.93, p<0.0001, n=15; Fig. S7). In early June, DIC concentrations were weakly positively correlated with CO_2 concentrations (R^2 = 0.24, p<0.0001, n=86; Fig. S5), however there was no discrepancy between water column and bottom water samples as it was observed in March samples. Overall, from March to June, mean DIC

concentrations in the bay area had declined to similar extends as CO_2 concentrations with on average 54% lower values at the river mouth and 25-5% lower values along the central axis of the bay area, which indicates that -irrespective of the temporal variability - there was an overall reduction in water column inorganic carbon within the bay in early June as compared to in March.

DO concentrations correlated negatively with CO_2 concentrations in early June. The strongest relationship (R^2 = 0.77, p < 0.001; n = 49) was found for data from June 2017, when maximum values in DO concentration (as well as saturation) coincided with minimum values in CO_2 concentrations near the location of the thermal bar (Fig. 2). During stratified conditions in June 2015 and 2016 , CO_2 and DO concentrations correlated negatively but to different degrees in epilimnetic (< 5 m depth; R^2 = 0.49, p < 0.001; n = 36;) and in hypolimnetic waters of the bay (R^2 = 0.41, p <0.001, n = 27).

Spatiotemporal variability in CO_2 fluxes

CO_2 fluxes from water to the atmosphere ranged from -44 to 162 mmol m^{-2} d^{-1} at actual wind speeds and from -16 and 62 mmol m^{-2} d^{-1} when k_{CO2} was calculated using the median wind speed of 4 m s^{-1} (Table 3). In the following, we refer for better comparability of the general patterns of CO_2 uptake and emission to the latter range of values.

The CO_2 emission from the bay during the 4-week mixing period after ice-melt in 2015 averaged 11 ± 4 (SD) mmol m^{-2} d^{-1}, which amounts to a total CO_2 loss of ~260 t C when extrapolated to the entire bay area. The CO_2 measurements during the 8-days mixing period in 2016, returned an average flux of 30 ± 5 mmol m^{-2} d^{-1} (see supplement). For comparison; integrating over the same time span of the first week of mixing after ice-melt in 2015 and 2016 the values from the two years return initial CO_2 losses of ~100 t C and of (at least) 180 t C, respectively. For comparison, CO_2 flux estimates for the central lake area were substantially lower with 2 to 7 mmol m^{-2} d^{-1} at ice breakup.

To assess the contribution of different sources to the CO_2 stored in the bay under ice (~1800 t C in mid-March 2016) and to the emission flux at ice-melt, we used the sediment and river datasets from 2016. Sediment incubation experiments returned CO_2 fluxes of 3.8 ± 2.0 mmol m^{-2} d^{-1} (Supplementary Information, Table S1), which matches with the trend observed by the deep water sensors in 2016 (4 μmol L^{-1} d^{-1}) as well as with values found in other studies addressing sediment CO_2 fluxes at cold and oxic conditions (Gudasz et al. 2010; MacIntyre et al. 2018). There were no significant differences between CO_2 fluxes in cores from the three sampling locations and we used

the average rate to estimate the magnitude of sediment CO_2 flux for the entire bay. This number equaled 3 t C d^{-1} (2-4 t C d^{-1}, 95% CI). Since the freeze up of the bay in early January, the water volume provided by the river accounted for about one third of the bay water volume (disregarding mixing of water masses with the central lake), and the CO_2 influx averaged 8 t C d^{-1} (7-10 t C d^{-1}) over this period. Together, these values indicate that the river and the sediments contributed 30-40% and 8-17%, respectively, to the total CO_2 content in the bay during the ice-covered period. However, the contribution of the river likely increased prior to ice-melt as the average river CO_2 influx increased to 22 t C d^{-1} (19-25 t C d^{-1}) during the month of April.

In early June, CO_2 fluxes varied between 6-32 mmol m^{-2} d^{-1} in the bay. Only one measurement point at the outer edge of the bay (PB3) in June 2016 revealed CO_2 uptake by the lake (-1 mmol m^2 d^{-1}), which indicates that this area was overall an emitter of CO_2 to the atmosphere during the spring season of the three years. Measurement points in the central lake revealed both uptake and emission flux during early June (-16 to 25 mmol m^{-2} d^{-1}). The two transects in June 2016 indicated a larger area of CO_2 uptake that extended from the shoreline northeast of the bay to the lake center (Fig. 5, -14 to 6 mmol m^{-2} d^{-1}; median: -5 mmol m^{-2} d^{-1}). In June 2017, in contrast, all measured locations in the central lake were emitting CO_2 (5-25 mmol m^{-2} d^{-1}). The lowest values from this range were obtained for sampling points near the thermal bar, where maxima in dissolved oxygen as well as in chlorophyll-a concentrations were observed (Table 1, Fig 2).

Discussion

The impact of river inflow on spatiotemporal CO_2 variability

Rivers tend to be more saturated in CO_2 than lakes and account for a significantly higher share of the global inland water CO_2 emission (Raymond et al. 2013; Lauerwald et al. 2015). However, while the hydrological control of CO_2 in lakes has been emphasized in various studies (e.g., Einola et al. 2011; McDonald et al. 2013; Weyhenmeyer et al. 2015), only limited knowledge exists about the riverine influence on the spatiotemporal variability of CO_2 in lakes over seasons and years (Pacheco et al. 2015), and particularly not over the ice-covered periods.

In support of our first hypothesis, the spatial dataset of Lake Onego revealed a substantially larger CO_2 variability in the river-impacted bay than in the central lake, with the most profound changes at the seasonal (i.e., from ice-covered to open-water periods) time-scale. Water at the river mouth was

406 2-6 times more saturated in CO_2 than the atmosphere which is similar to the range of values observed
407 in other large boreal rivers (Campeau and Del Giorgio 2014). Water in the central lake, in contrast,
408 maintained CO_2 concentrations around atmospheric equilibrium concentrations, which is lower than
409 median values (540-980 µatm) reported for 37 large boreal lakes in Finland during the winter,
410 summer, and autumn season (Rantakari and Kortelainen 2005). The Shuya river was the main driver
411 of the spatial configuration of CO_2, DOC, and DIC concentrations in the PB area, with the most
412 apparent influence during the winter period. The vertical and horizontal concentration gradients,
413 which developed during low discharge conditions from the river mouth towards the central lake,
414 reflect the intrusion and gradual mixing of CO_2- and DOC-rich river water with the more diluted
415 water of the lake. DIC concentration gradients showed an opposite pattern to those of CO_2 and DOC
416 over most of the water column, due to the lower DIC content in the river than in the lake water (Fig.
417 2 and Fig. S3).

418 The CO_2 concentration in bottom waters of the bay, in contrast, was controlled by CO_2 diffusing from
419 the sediments as indicated by the high CO_2 concentration values and the positive correlation of CO_2
420 with DIC in these layers (Figs. 2,3,4, and Supplementary Information, Fig. S7). Our calculations from
421 the 2016 dataset demonstrate that riverine CO_2 flux was about twice as important for the under-ice
422 CO_2 budget of the bay as the sediment CO_2 flux. One hand, this ratio is likely to deviate between
423 years with different discharge conditions, however, on the other hand the contribution of CO_2 by
424 respiration in sediments may also be seen as an indirect influence of the river inflow. About 60% of
425 the organic matter in PB originates from terrestrial sources and the bay area also acts as the primary
426 deposition site for river particles (Sabylina et al. 2010). We therefore conclude that CO_2 dynamics
427 under ice and the emission flux at ice-melt from this bay are largely driven by river inflow, and that
428 similar condition could apply to several of the other bays in the north of PB. For instance, the 225
429 km^2 large bay of Kondopoga and the 80 km^2 large bay of Lizhma exhibit a similar mean depth as PB
430 and receive water from two of the major tributaries of the lake (Podsechin et al. 2009; Sabylina et al.
431 2010). The spatial footprint of riverine CO_2, however, will vary with local morphometry and flow
432 conditions, and it is therefore difficult to extrapolate from the PB area to other river inflow sites.
433 However, regardless of the site-specific flow patterns, all tributaries together will deliver large
434 quantities of CO_2 to the lake. It has been shown that fluvial organic matter inputs scale proportionally
435 with discharge around the lake such that comparable conditions can be anticipated for CO_2 (Sabylina
436 et al. 2010). Taking into account both spatial and temporal differences in CO_2 concentrations of the
437 bay and the central lake at ice-melt in 2015 and 2016, indicates that the PB area emitted 8 (2-15, 95%

CI) times as much CO_2 as an equally-sized area in the central lake, which illustrates the need to integrate the various inflow regions when quantifying CO_2 emission from this large system.

The spatial variability of CO_2 in early June displayed a highly different pattern from the conditions found in March under ice. (Figs. 2, 3 and Supplementary Information, Fig. S7). After river discharge had peaked in April and May, both CO_2 and DIC concentrations at the river mouth showed a considerable decrease of ~50%, compared to the values obtained in March, which was probably related to a dilution effect during snowmelt and to decreased DIC export from soils (Kokic et al. 2015). DOC concentrations at the river mouth, in contrast, did not differ between seasons, which might be explained by the fact that DIC and DOC can be exported from different soil horizons during varying runoff conditions (Giesler et al. 2014; Nydahl et al. 2017). However, despite the difference in DOC and DIC changes, both their spatial gradients indicated the path of river intrusion up to 15 km past the bay area in early June. The spatial configuration of CO_2, however, was disconnected from this pattern and CO_2 concentrations correlated with DO concentrations instead (Fig. 2). Together with observed maxima in chlorophyll-a concentrations in surface waters and at the thermal bar, these pattern demonstrate that biological processes (phytoplankton growth and organic matter breakdown) interfered the physically driven CO_2 signal from the river during this time of the year (Figs. 2, 3; Table 1).

Drivers of interannual CO_2 variability

The bay acted per m^2 as a consistently higher CO_2 source to the atmosphere than the central lake, which confirms our second hypothesis. However, there were also large interannual differences in the overall spring CO_2 emission from this region. First, our spatiotemporal CO_2 dataset from the ice-covered periods shows that mean water column CO_2 concentrations in the bay were 37-58% lower in March 2015 than in March 2016 and 2017. This lower CO_2 content could be explained by the 50% lower discharge rates during winter 2015 and these in turn to lower amounts of precipitation (Fig. S3). However, while precipitation was overall lower in 2015 than in the two following years (both at the seasonal and annual time scale; Fig. S3) we could not detect any clear relationship in the long-term discharge and precipitation dataset. Nevertheless, the precipitation data of the three study years reveal a considerably wetter spring in comparison to the previous decade; and several studies have shown that fluvial carbon export from soils and the CO_2 emission from rivers and lakes may correlate positively with annual precipitation (Kelly et al. 2001; Rantakari and Kortelainen 2005; Butman and

Raymond 2011; Öquist et al. 2014). It is therefore vital to capture such interannual differences in CO_2 dynamic and their controls at river-inflow sites.

Second, the temporal courses of CO_2 measured *in-situ* in 2015 and 2016 supports the recent findings that CO_2 does not necessarily accumulate linearly and homogenously distributed under ice but that convective mixing patterns play an important role for CO_2 distribution and emission at ice-melt (Denfeld et al. 2015b, 2018; Pasche et al. 2019). This shows that the interplay of variation in discharge with hydrodynamic conditions under ice have a strong influence on CO_2 dynamics and drive the interannual variability in CO_2 emission flux at ice-melt. In this context, Pacheco et al. (2015) showed that variations in river intrusion depth can determine wether CO_2 is evaded directly into the atmophere during overflow, or dilutes within the water column during underflow conditions. This finding has important implications for assumptions made about CO_2 release at ice melt in large-scale CO_2 emission estimates (Cole et al. 2007; Raymond et al. 2013; Hastie et al. 2017).
Although we could not calculate the emission flux for the entire ice-melt period in 2016, due to the CO_2 sensor failure at 4.5 m water depth, the comparison of flux values for the first week of mixing after ice-break in suggests that CO_2 emission was about twice as higher in 2016 than in 2015. There were no in-situ sensor CO_2 records available for the ice-melt and spring mixing period of 2017, however, CO_2 conditions in March 2017 were similar to those in March 2016, and the low water temperatures of the bay in June 2017 indicate that mixing period probably lasted longer than in 2016. Furthermore, CO_2 emission in early June were still considerably higher in 2017 (20 ± 2 mmol m^{-2} d^{-1}) than in 2016 (12 ± 3 mmol m^{-2} d^{-1}). We therefore conclude that the CO_2 emission during spring mixing in 2017 exceeded the emission of the two previous years.

Third, we found large interannual differences in the CO_2 conditions in early June, which can be related to the variable climate of the three spring seasons (Fig S3). Air temperature data revealed an unusual warm and a comparatively cold period after ice-melt in 2016 and 2017, respectively, with consequences for the duration of the mixing period and the development of summer stratification in the lake. The more stable stratification in 2016 may have supported an earlier occurrence of phytoplankton spring blooms that decreased CO_2 values in surface waters during this year (Figs. 2 and S6). The cold and wet spring of 2017 on the contrary resulted in lower water temperatures and a closer proximity of the thermal bar to the bay area, which impacted spring bloom dynamics and subsequently the spatiotemporal CO_2 variability. The conditions during spring 2015 can be seen as an intermediate stage in comparison to the conditions of the other two years. The results reveal that the timing of sampling in relation to the varying spring conditions are crucial for estimating CO_2

fluxes during this time of the year. Continuous, long-term sampling is required to capture such temporal variations, especially during the critical period of ice melt.

Climate warming has implications for the hydrological connectivity between aquatic ecosystems on multiple levels. With shorter ice-cover seasons, earlier onsets of summer stratification, and changing precipitation patterns in northern latitudes, it is vital to understand the mechanisms and their interplay that control CO_2 dynamics in these systems (De Stasio et al. 1996; Lopez et al. 2019). The PB area has lost 20 days of lake-ice cover on average over the past 60 years (Filatov et al. 2019). If this trend persists the ice-covered period might decrease from 5 to less than 3 month by the end of the 21st centur. Furthermore, long-term data of the Shuya river indicate that discharge has been increasing since 1991 during winter months (Filatov et al. 2019). Resolving CO_2 variability in river inflow areas is vital to assess linkages and bottlenecks between systems. Further studies also at other river-inflow areas and over the entire annual cycle are needed in order to capture the whole range of CO_2 variability at these sites and to predict their role in whole-lake CO_2 fluxes under global change.

Conclusions

The ice-melt period is a critical time window for CO_2 emission from lakes, however, large-scale estimates presently do not resolve temporal variability and spatial gradients in CO_2 for such systems at all. Our CO_2 dataset for Lake Onego, the second largest lake in Europe, demonstrates large seasonal and interannual differences in CO_2 concentration in a river-impacted bay region and indicates conditions under which substantial parts of the lake can be turned from a CO_2 sink into a CO_2 source at ice-melt. We conclude that the boundaries between aquatic sub-systems (e.g., between river, bay and open lake areas) are highly dynamic in space and time and that resolving these dynamics is crucial to quantify and predict CO_2 emission from large lakes more accurately. Such efforts, however, can only be achieved by integral measurements or modelling of spatial, seasonal, and interannual variability of CO_2 concentrations and fluxes. For future research on large-scale CO_2 flux dynamics, we recommend to better integrate near-shore areas of large lakes because these may add comparatively more uncertainty to whole-lake CO_2 emission estimates than more remote locations.

Acknowledgments

The authors thank the Limnology at EPFL, and the NWPI at the Russian Academy of Sciences in Karelia, for their logistic and technical support during field campaigns. We especially thank Nikolay

535 Filatov, Roman Zdorovennov, Vasily Kovalenko for the excellent coordination and Sébastian
536 Lavanchy for technical support of CO_2 measurements. The authors also thank AuA laboratory at
537 Eawag for the analyses of DOC samples. This research was funded by the "Fondation pour l'Etude
538 des Eaux du Léman" as part of the "Life under ice" project, which took place at Lake Onego from
539 2015 to 2017. Finally the authors would like to express their thanks to three anonymous reviewers
540 for their valuable feedback on the earlier manuscript version.
541

542 **References**

543

544 Aufdenkampe, A. K., E. Mayorga, P. a Raymond, J. M. Melack, S. C. Doney, S. R. Alin, R. E. Aalto,
545 and K. Yoo. 2011. Riverine coupling of biogeochemical cycles between land, oceans, and
546 atmosphere. Front. Ecol. Environ. **9**: 53–60. doi:10.1890/100014
547 Baehr, M. M., and M. D. Degrandpre. 2002. Under-ice CO 2 and O 2 variability in a freshwater lake.
548 Biogeochemistry **61**: 95–113.
549 Baehr, M. M., and M. D. Degrandpre. 2004. In situ pCO2 and O2 measurements in a lake during
550 turnover and stratification: Observations and modeling. Limnol. Oceanogr. **49**: 330–340.
551 Butman, D., and P. A. Raymond. 2011. Significant efflux of carbon dioxide from streams and rivers
552 in the United States. Nat. Geosci. **4**: 839–842. doi:10.1038/ngeo1294
553 Campeau, A., and P. A. Del Giorgio. 2014. Patterns in CH4 and CO2 concentrations across boreal
554 rivers: Major drivers and implications for fluvial greenhouse emissions under climate change
555 scenarios. Glob. Chang. Biol. **20**: 1075–1088. doi:10.1111/gcb.12479
556 Chmiel, H. E., J. Kokic, B. A. Denfeld, and others. 2016. The role of sediments in the carbon budget
557 of a small boreal lake. Limnol. Oceanogr. **61**: 1814–1825. doi:10.1002/lno.10336
558 Cole, J. J., and N. F. Caraco. 1998. Atmospheric exchange of carbon dioxide in a low-wind
559 oligotrophic lake measured by the addition of SF6. Limnol. Oceanogr. **43**: 647–656.
560 doi:10.4319/lo.1998.43.4.0647
561 Cole, J. J., Y. T. Prairie, N. F. Caraco, and others. 2007. Plumbing the Global Carbon Cycle:
562 Integrating Inland Waters into the Terrestrial Carbon Budget. Ecosystems **10**: 172–185.
563 doi:10.1007/s10021-006-9013-8
564 Crawford, J. T., N. R. Lottig, E. H. Stanley, J. F. Walker, P. C. Hanson, J. C. Finlay, and R. G.
565 Striegl. 2014. CO2 and CH4 emissions from streams in a lake-rich landscape: Patterns, control,
566 and regional significance. Global Biogeochem. Cycles **28**: 1–14.
567 doi:10.1002/2013GB004661.Received
568 Crusius, J., and R. Wanninkhof. 2003. Gas transfer velocities measured at low wind speed over a lake.
569 Limnol. Oceanogr. **48**: 1010–1017. doi:10.4319/lo.2003.48.3.1010
570 Denfeld, B. A., H. M. Baulch, P. A. del Giorgio, S. E. Hampton, and J. Karlsson. 2018. A synthesis of

carbon dioxide and methane dynamics during the ice-covered period of northern lakes. Limnol. Oceanogr. Lett. doi:10.1002/lol2.10079

Denfeld, B. A., M. B. Wallin, E. Sahlée, S. Sobek, J. Kokic, H. E. Chmiel, and G. A. Weyhenmeyer. 2015a. Temporal and spatial carbon dioxide concentration patterns in a small boreal lake in relation to ice cover dynamics. Boreal Environ. Res. **20**: 679–692.

Denfeld, B. A., M. B. Wallin, E. Sahlée, S. Sobek, J. Kokic, H. E. Chmiel, and G. A. Weyhenmeyer. 2015b. Temporal and spatial carbon dioxide concentration patterns in a small boreal lake in relation to ice cover dynamics. Boreal Environ. Res. **20**: 1–14.

Efremova, T. A., A. V Sabylina, P. A. Lozovik, V. I. Slaveykova, M. V Zobkova, and N. Pasche. 2019. Seasonal and spatial variation in hydrochemical parameters for Lake Onego (Russia): Insights from 2016 field monitoring. Inl. Waters accepted.

Einola, E., M. Rantakari, P. Kankaala, P. Kortelainen, A. Ojala, H. Pajunen, S. Mäkelä, and L. Arvola. 2011. Carbon pools and fluxes in a chain of five boreal lakes: A dry and wet year comparison. J. Geophys. Res. Biogeosciences **116**: 1–13. doi:10.1029/2010JG001636

Filatov, N. N., V. Baklagin, T. Efremova, L. Nazarova, and N. Palshin. 2019. Climate change impacts on the watersheds of Lakes Onego and Ladoga from remote sensing and in situ data. Inl. Waters **Accepted**.

Giesler, R., S. W. Lyon, C. M. Mörth, J. Karlsson, E. M. Karlsson, E. J. Jantze, G. Destouni, and C. Humborg. 2014. Catchment-scale dissolved carbon concentrations and export estimates across six subarctic streams in northern Sweden. Biogeosciences **11**: 525–537. doi:10.5194/bg-11-525-2014

Gudasz, C., D. Bastviken, K. Steger, K. Premke, S. Sobek, and L. J. Tranvik. 2010. Temperature-controlled organic carbon mineralization in lake sediments. Nature **466**: 478–481. doi:10.1038/nature09383

Hastie, A., R. Lauerwald, G. Weyhenmeyer, S. Sobek, C. Verpoorter, and P. Regnier. 2017. CO2 evasion from boreal lakes: Revised estimate, drivers of spatial variability, and future projections. Glob. Chang. Biol. **2**: 1–18. doi:10.1111/gcb.13902

Intergovernmental Panel on Climate Change (IPCC). 2013. Climate Change 2013: The Physical Science Basis. Working Group I Contribution to the Fifth Assessment Report of the Intergovernmental Panel on Climate Change Rep, Cambridge Univ. Press.

Jones, J. B. J., and P. J. Mulholland. 1998. Carbon Dioxide Variation in a Hardwood Forest Stream: An Integrative Measure of Whole Catchment Soil Respiration. Ecosystems **1**: 183–196.

Jones, J. R., D. V. Obrecht, J. L. Graham, M. B. Balmer, C. T. Filstrup, and J. A. Downing. 2016. Seasonal patterns in carbon dioxide in 15 mid-continent (USA) reservoirs. Inl. Waters **6**: 265–272. doi:10.5268/IW-6.2.982

Karlsson, J., R. Giesler, J. Persson, and E. Lundin. 2013. High emission of carbon dioxide and methane during ice thaw in high latitude lakes. Geophys. Res. Lett. **40**: 1123–1127.

608 doi:10.1002/grl.50152
609 Kelly, C. a., E. Fee, P. S. Ramlal, J. W. M. Rudd, R. H. Hesslein, C. Anema, and E. U. Schindler.
610 2001. Natural variability of carbon dioxide and net epilimnetic production in the surface waters
611 of boreal lakes of different sizes. Limnol. Oceanogr. **46**: 1054–1064.
612 doi:10.4319/lo.2001.46.5.1054
613 Klaus, M., D. A. Seekell, W. Lidberg, and J. Karlsson. 2019. Evaluations of climate and land
614 management effects on lake carbon cycling need to account for temporal variability in CO_2
615 concentrations. Global Biogeochem. Cycles. doi:10.1029/2018GB005979
616 Kokic, J., M. B. Wallin, H. E. Chmiel, B. A. Denfeld, and S. Sobek. 2015. Carbon dioxide evasion
617 from headwater systems strongly contributes to the total export of carbon from a small boreal
618 lake catchment. J. Geophys. Res. Biogeosciences **120**: 13–28. doi:10.1002/2014JG002706
619 Lauerwald, R., G. G. Laruelle, J. Hartmann, P. Ciais, and P. A. G. Regnier. 2015. Spatial patterns in
620 CO2 evasion from the global river network. Global Biogeochem. Cycles **29**: 534–554.
621 doi:10.1002/ 2014GB004941.
622 Liss, P. S., and L. Merlivat. 1986. Air-Sea Gas Exchange Rates: Introduction and Synthesis, *In* In:
623 Buat-Ménard P. (eds) The Role of Air-Sea Exchange in Geochemical Cycling. NATO ASI
624 Series (Series C: Mathematical and Physical Sciences), vol 185. Springer, Dordrecht.
625 Liss, P. S., and P. G. Slater. 1974. Flux of gases across the Air-Sea interface. Nature **247**: 181–184.
626 doi:10.1038/247181a0
627 Lopez, L. S., B. A. Hewitt, and S. Sharma. 2019. Reaching a breaking point: How is climate change
628 influencing the timing of ice breakup in lakes across the northern hemisphere? Limnol.
629 Oceanogr. 1–11. doi:10.1002/lno.11239
630 Lozovik, P. A., A. K. Morozov, M. B. Zobkov, T. A. Dukhovicheva, and L. A. Osipova. 2007.
631 Allochthonous and autochthonous organic matter in surface waters in Karelia. Water Resour. **34**:
632 204–216. doi:10.1134/S009780780702011X
633 Maberly, S. C., P. A. Barker, A. W. Stott, and M. M. De Ville. 2013. Catchment productivity controls
634 CO2 emissions from lakes. Nat. Clim. Chang. **3**: 391–394. doi:10.1038/nclimate1748
635 MacIntyre, S., A. Cortés, and S. Sadro. 2018. Sediment respiration drives circulation and production
636 of CO 2 in ice-covered Alaskan arctic lakes . Limnol. Oceanogr. Lett. **3**: 302–310.
637 doi:10.1002/lol2.10083
638 McDonald, C. P., E. G. Stets, R. G. Striegl, and D. Butman. 2013. Inorganic carbon loading as a
639 primary driver of dissolved carbon dioxide concentrations in the lakes and reservoirs of the
640 contiguous United States. Global Biogeochem. Cycles **27**: 285–295. doi:10.1002/gbc.20032
641 Natchimuthu, S., I. Sundgren, M. Gålfalk, L. Klemedtsson, and D. Bastviken. 2017. Spatiotemporal
642 variability of lake pCO2 and CO2 fluxes in a hemiboreal catchment Sivakiruthika. J. Geophys.
643 Res. Biogeosciences **122**: 30–49. doi:10.1002/2016JG003449.
644 Nydahl, A. C., M. B. Wallin, and G. A. Weyhenmeyer. 2017. No long-term trends in pCO2 despite

increasing organic carbon concentrations in boreal lakes, streams, and rivers. Global Biogeochem. Cycles **31**: 985–995. doi:10.1002/2016GB005539

Öquist, M. G., K. Bishop, A. Grelle, L. Klemedtsson, H. Laudon, A. Lindroth, M. B. Wallin, and M. B. Nilsson. 2014. The Full Annual Carbon Balance of Boreal Forests Is Highly Sensitive to Precipitation. Environ. Sci. Technol.

Öquist, M. G., M. Wallin, J. Seibert, K. Bishop, and H. Laudon. 2009. Dissolved inorganic carbon export across the soil/stream interface and its fate in a boreal headwater stream. Environ. Sci. Technol. **43**: 7364–7369. doi:10.1021/es900416h

Pacheco, F. S., M. C. S. Soares, A. T. Assireu, M. P. Curtarelli, G. Abril, J. L. Stech, P. C. Alvalá, and J. P. Ometto. 2015. The effects of river inflow and retention time on the spatial heterogeneity of chlorophyll and water-air CO2 fluxes in a tropical hydropower reservoir. Biogeosciences **12**: 147–162. doi:10.5194/bg-12-147-2015

Paranaíba, J. R., N. Barros, R. Mendonça, A. Linkhorst, A. Isidorova, F. Roland, R. M. Almeida, and S. Sobek. 2018. Spatially Resolved Measurements of CO2 and CH4 Concentration and Gas-Exchange Velocity Highly Influence Carbon-Emission Estimates of Reservoirs. Environ. Sci. Technol. **52**: 607–615. doi:10.1021/acs.est.7b05138

Pasche, N., H. Hofmann, D. Bouffard, C. J. Schubert, P. A. Lozovik, and S. Sobek. 2019. Implications of river intrusion and convective mixing on the spatial and temporal variability of under-ice CO2. Inl. Waters **Accepted**.

Podsechin, V., H. Kaipainen, N. Filatov, T. Frisk, A. Paananen, A. Terzhevik, and H. Vuoristo. 2009. Development of Water Protection of Lake Onega. Finnish Environ. **36**: 0–39.

Rantakari, M., and P. Kortelainen. 2005. Interannual variation and climatic regulation of the CO2 emission from large boreal lakes. Glob. Chang. Biol. **11**: 1368–1380. doi:10.1111/j.1365-2486.2005.00982.x

Raymond, P. a, J. Hartmann, R. Lauerwald, and others. 2013. Global carbon dioxide emissions from inland waters. Nature **503**: 355–9. doi:10.1038/nature12760

Sabylina, A. V., P. a. Lozovik, and M. B. Zobkov. 2010. Water chemistry in Onega Lake and its tributaries. Water Resour. **37**: 842–853. doi:10.1134/S0097807810060102

Schilder, J., D. Bastviken, M. van Hardenbroek, P. Kankaala, P. Rinta, T. Stötter, and O. Heiri. 2013. Spatial heterogeneity and lake morphology affect diffusive greenhouse gas emission estimates of lakes. Geophys. Res. Lett. **40**: 5752–5756. doi:10.1002/2013GL057669

Sobek, S., G. Algesten, A. K. Bergström, M. Jansson, and L. J. Tranvik. 2003. The catchment and climate regulation of pCO2 in boreal lakes. Glob. Chang. Biol. **9**: 630–641. doi:10.1046/j.1365-2486.2003.00619.x

De Stasio, B. T., D. K. Hill, J. M. Kleinhans, N. P. Nibbelink, and J. J. Magnuson. 1996. Potential effects of global climate change on small north-temperate lakes: Physics, fish, and plankton. Limnol. Oceanogr. **41**: 1136–1149. doi:10.4319/lo.1996.41.5.1136

Teodoru, C. R., Y. T. Prairie, and P. A. del Giorgio. 2011. Spatial Heterogeneity of Surface CO2 Fluxes in a Newly Created Eastmain-1 Reservoir in Northern Quebec, Canada. Ecosystems **14**: 28–46. doi:10.1007/s10021-010-9393-7

Tranvik, L. J., J. A. Downing, J. B. Cotner, and others. 2009. Lakes and reservoirs as regulators of carbon cycling and climate. Limnol. Oceanogr. **54**: 2298–2314. doi:10.4319/lo.2009.54.6_part_2.2298

Verpoorter, C., T. Kutser, D. a. Seekell, and L. J. Tranvik. 2014. A Global Inventory of Lakes Based on High-Resolution Satellite Imagery. Geophys. Res. Lett. **41**: 6396–6402. doi:10.1002/2014GL060641

Wallin, M. B., T. Grabs, I. Buffam, H. Laudon, A. Ågren, M. G. Öquist, and K. Bishop. 2013. Evasion of CO2 from streams - The dominant component of the carbon export through the aquatic conduit in a boreal landscape. Glob. Chang. Biol. **19**: 785–797. doi:10.1111/gcb.12083

Wanninkhof, R. H. 1992. Relationship between wind speed and gas exchange. J. Geophys. Res. **97**: 7373–7382. doi:10.1029/92JC00188

Weiss, R. F. 1974. Carbon dioxide in water and seawater: the solubility of a non-ideal gas. Mar. Chem. **2**: 203–215.

Weyhenmeyer, G. a., P. Kortelainen, S. Sobek, R. Müller, and M. Rantakari. 2012. Carbon Dioxide in Boreal Surface Waters: A Comparison of Lakes and Streams. Ecosystems **15**: 1295–1307. doi:10.1007/s10021-012-9585-4

Weyhenmeyer, G. A., S. Kosten, M. B. Wallin, L. J. Tranvik, E. Jeppesen, and F. Roland. 2015. Significant fraction of CO2 emissions from boreal lakes derived from hydrologic inorganic carbon inputs. Nat. Geosci. **8**: 933–936. doi:10.1038/NGEO2582

Weyhenmeyer, G. A., D. M. Livingstone, M. Meili, O. Jensen, B. Benson, and J. J. Magnuson. 2011. Large geographical differences in the sensitivity of ice-covered lakes and rivers in the Northern Hemisphere to temperature changes. Glob. Chang. Biol. **17**: 268–275. doi:10.1111/j.1365-2486.2010.02249.x

Wiesenburg, D. A., and N. L. Guinasso. 1979. Equilibrium Solubilities of Methane, Carbon Monoxide, and Hydrogen in Water and Sea Water. J. Chem. Eng. Data **24**: 356–360. doi:10.1021/je60083a006

Worrall, F., and A. Lancaster. 2005. The Release of CO2 from Riverwaters – the Contribution of Excess CO2 from Groundwater. Biogeochemistry **76**: 299–317. doi:10.1007/s10533-005-6449-4

Figure captions

Fig. 1: Geographic location and bathymetric map of Lake Onego including sampling stations (red stars) and surface measurements along transect during ice-free conditions in June 2016 (TS, yellow dots; TB, orange dots) and in June 2017 (T0, purple dots).

Fig. 2: Transects of water temperature (°C), dissolved oxygen saturation (%), CO_2 concentrations (µmol L^{-1}) , DIC and DOC concentrations (mmol L^{-1}) between the entry of the Shuya river and the central basin of Lake Onego, measured in June 2015 (left panel), 2016 (center panel), and 2017 (right panel). Dashed black lines indicate the transition from the Bay of Petrozavodsk to the central main basin. The dashed white lines mark the location of the thermal bar in June 2017.

Fig. 3: CO_2 concentration (µmol L^{-1}), DIC and DOC concentration (mmol L^{-1}) along the sampling stations between the entry of the Shuya River (RS) and the transition of Petrozavodsk Bay to the central basin of Lake Onego (PB3), measured during ice-cover periods in March 2016 (left panel) and 2017 (right panel).

Fig. 4: Temporal course of CO_2 concentrations (µmol L^{-1}) at 3/4.5 m (surface, black line) and at 25/26 m (near-bottom, grey line) water depth in 2015 (a) and 2016 (b). The periods of ice cover are indicated by darker shaded areas and the ice break-up period by lighter shaded areas. The vertical dashed lines show the beginning of the stratified period. Note the log scale on the y-axis**.**

Fig. 5: Lateral variability in CO_2 flux to the atmosphere (mmol m^{-2} d^{-1}) in the Bay of Petrozavodsk and the central basin of Lake Onego on 3rd-7th June 2016. Fluxes were calculated using the median wind speed (4 m s^{-1}) over the area. Sampling stations are marked as open circles.

Figures

Fig. 1:

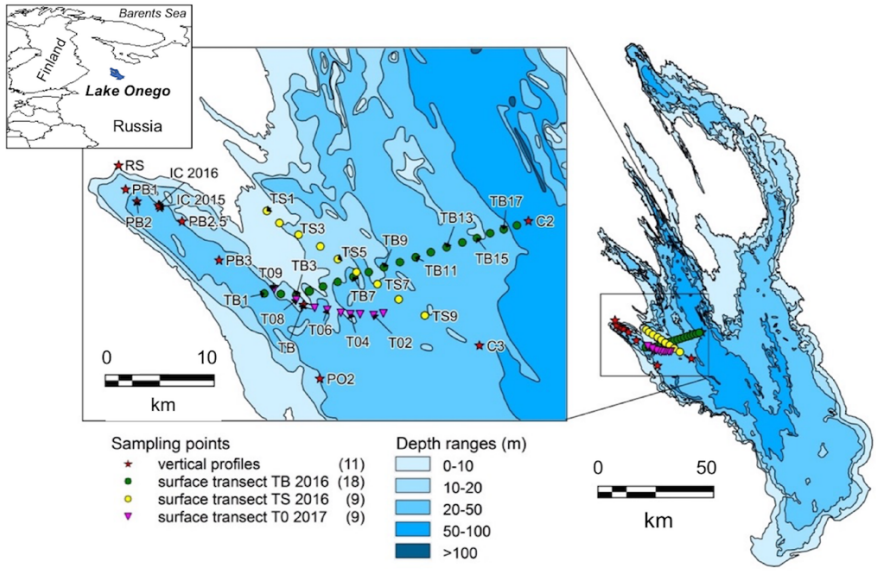

742 **Fig. 2:**

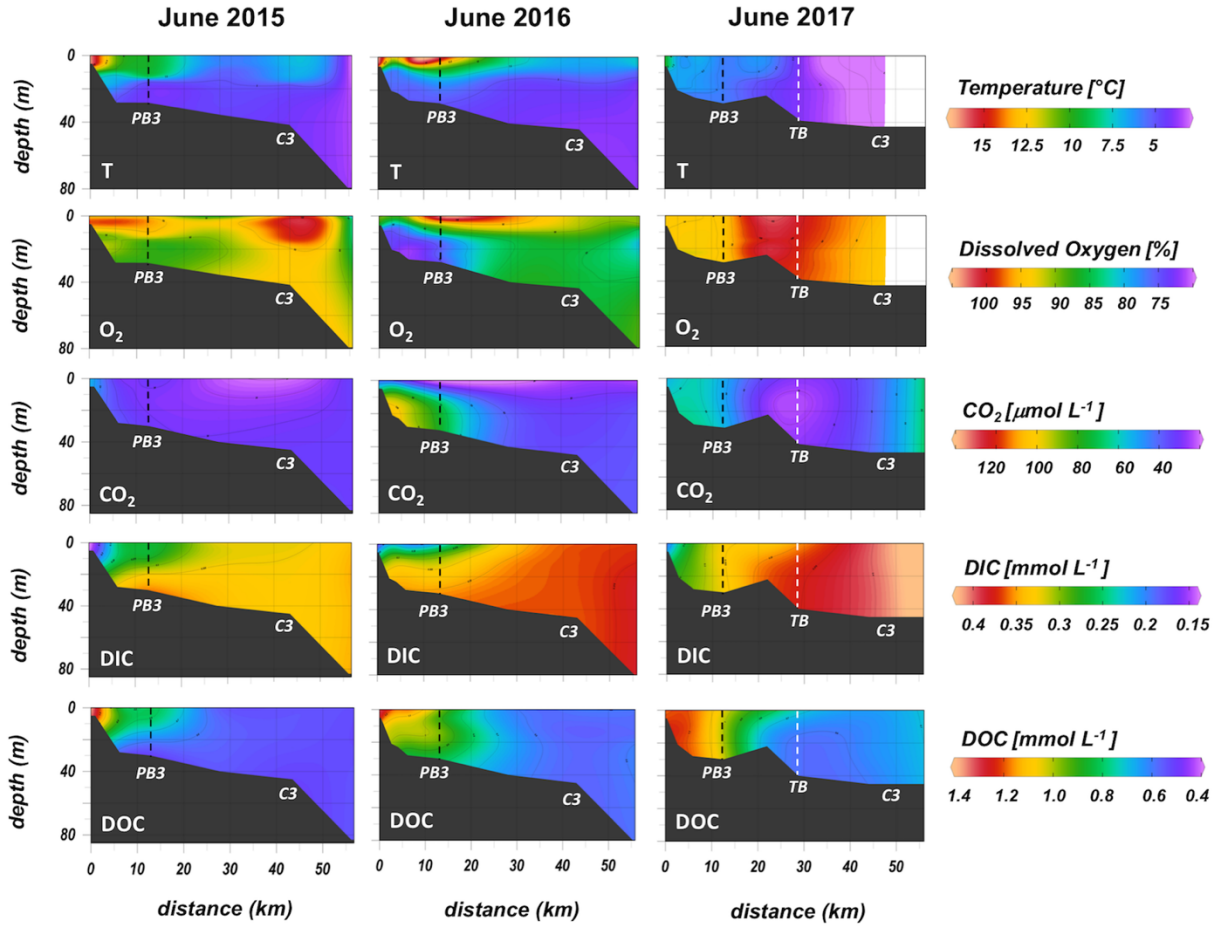

743

744 **Fig. 3:**

745

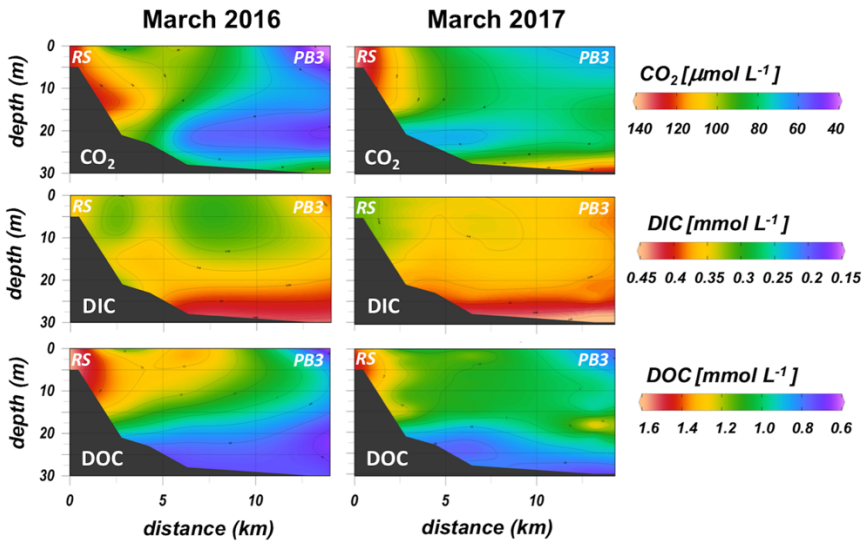

746

747

748 **Fig. 4:**

749

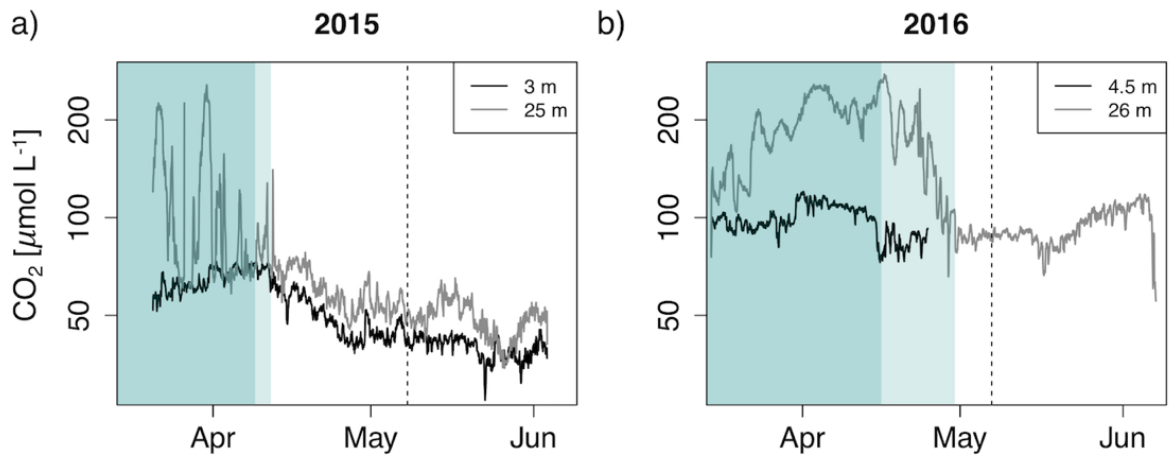

750

751 **Fig. 5:**

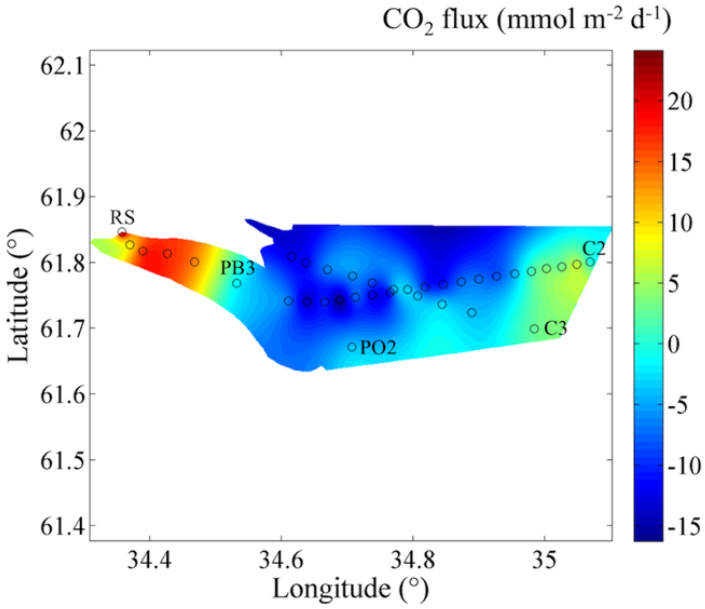

752

753

754

755

756

757

758

759

760

761

762 **Tables**

763

764 **Table 1:** Nutrient and chlorophyll-a contents at the Shuya River mouth and in Lake Onego.
765 Nutrient values are given as mean water column concentrations and chlorophyll-a as the total
766 concentration range obtained during winter and spring sampling campaigns from 2015-2017
767 (Efremova et al. 2019, Suarez et al. 2019).

768

Site	Z_{max} [m]	**TN** [mg L^{-1}]	**TP** [µg L^{-1}]	**chlorophyll-a** [µg L^{-1}]
Shuya River mouth	5	0.52-1.04	35-37	-
Bay of Petrozavodsk	27	0.44-0.51	20-23	0.5-6.1
Central lake basin	127	0.37-0.40	6-8	0.5-1.5*
Thermal bar (2017)	21	-	-	4.4-8.9*

769

770 *June data only

771

772

773

774

775

776

777

778

779

780

781

782

783

Table 2: Water column CO_2, DIC, and DOC concentrations for several stations in Lake Onego, obtained from vertical profiles in March and June 2015, 2016, and 2017. Values denote mean and standard deviation of linearly interpolated profile data.

Location	**CO_2 [µmol L^{-1}]**		**DIC [mmol L^{-1}]**		**DOC [mmol L^{-1}]**	
Year	March	June	March	June	March	June
River Shuya						
2015	120	52	0.33	0.14	1.18	1.33
2016	129	45	0.29	0.17	1.54	1.34
2017	131	52	0.31	0.15	1.58	1.50
PB-1						
2015	n.d.	n.d.	n.d.	n.d.	n.d.	n.d.
2016	104 ± 17	86 ± 19	0.21 ± 0.02	0.31 ± 0.03	1.24 ± 0.13	1.04 ± 0.06
2017	97 ± 14	62 ± 1	0.35 ± 0.02	0.27 ± 0.00	1.11 ± 0.09	1.23 ± 0.03
IC (bay centre)						
2015	52 ± 23	34 ± 3	0.37 ± 0.04	0.28 ± 0.03	0.67 ± 0.03	0.79 ± 0.10
2016	82 ± 18	81 ± 21	0.22 ± 0.02	0.30 ± 0.06	1.07 ± 0.02	1.02 ± 0.15
2017	79 ± 7	62 ± 1	0.37 ± 0.02	0.28 ± 0.00	0.97 ± 0.12	1.20 ± 0.02
PB-3						
2015	n.d.	30 ± 1	n.d.	0.30 ± 0.04	n.d.	0.73 ± 0.11
2016	66 ± 29	62 ± 23	0.36 ± 0.02	0.31 ± 0.04	0.83 ± 0.13	0.99 ± 0.07
2017	85 ± 23	52 ± 1	0.39 ± 0.04	0.32 ± 0.00	0.98 ± 0.12	0.96 ± 0.13
C3 (open lake)						
2015	35 ± 3	27 ± 4	0.36 ± 0.01	0.33 ± 0.00	n.d.	0.80 ± 0.07
2016	35 ± 4	34 ± 3	0.21 ± 0.01	0.36 ± 0.00	0.73 ± 0.02	0.58 ± 0.02
2017	n.d.	39 ± 0	n.d.	0.40 ± 0.00	n.d.	0.36 ± 0.02

799 **Table 3:** Range in surface water CO_2 concentration, CO_2 flux, and water temperature in Lake
800 Onego during June 2015, 2016, and 2017

Location	**CO_2 [µmol L^{-1}]**	**CO_2 flux [mmol m^{-2} d^{-1}]**			**T [°C]**
Year		*C&C 1998*	*C&W 2003*	*Mean at 4 m s^{-1}*	
Petrozavodsk Bay					
2015	29-52 (*n*=3)	8-71	13-161	6-32	9.3-16.2
2016	31-45 (*n*=5)	-1-26	0-24	-1-25	10.9-16.1
2017	51-63 (*n*=4)	19-69	11-162	17-26	5.9-9.2
Central lake basin					
2015	20-33 (*n*=3)	-1-4	-2-4	-1-4	3.6-6.9
2016	1-30 (*n*=32)	-21-9	-44-21	-16-6	7.1-16.7
2017	33-62 (*n*=11)	5-42	9-96	5-25	2.5-6.0

801
802